ACADEMIA ROMÂNĂ
Revue Roumaine de Chimie
https://www.icf.ro/rrch/

Rev. Roum. Chim.,
2023, *68*(7–8), 327–337
DOI: 10.33224/rrch.2023.68.7-8.02

Dedicated to Dr. Niculae I. Ionescu
on the occasion of his 90th anniversary

NONIONIC SURFACTANT-TEMPLATED MESOPOROUS SILICA AS SUPPORTS FOR NICKEL ACTIVE CATALYSTS IN LIQUID PHASE ORGANIC COMPOUNDS OXIDATION

Marieta BALCAN, Dan F. ANGHEL, Daniela NEGOESCU, Veronica BRATAN and Viorica PARVULESCU*

"Ilie Murgulescu" Institute of Physical Chemistry, Roumanian Academy, Spl. Independentei 202, 060021 Bucharest, Roumania

Received November 25, 2022

Three surfactants were selected from a series of $EO_x/PO_y/EO_x$ triblock copolymers and ethoxylated octylphenol as nonionic templating agents for the synthesis of silica mesoporous materials at room temperature and by hydrothermal treatment. The surfactants were ethylene oxide-propylene oxide-ethylene oxide tri-block copolymers (Pluronic F68) and a polydisperse ethoxylated octylphenol (Triton X-100). The obtained materials were compared with SBA-15 mesoporous silica synthesized with Pluronic P123 surfactant and were used as support to obtain Ni and NiTi-silica catalysts (2.5% NiO, 5% TiO_2). The synthesized materials were characterized by X-ray diffraction, scanning electron microscopy (SEM), transmission electron microscopy (TEM), N_2 adsorption-desorption, IR and UV-Vis spectroscopy. Catalytic and photocatalytic activity of Ni and NiTi-silica samples were tested, with and without H_2O_2, for phenol and Brilliant Blue FCF dye oxidative degradation in the liquid phase. The obtained results showed a significant effect of surfactant on silica structure, morphology, texture, catalytic and photocatalytic properties.

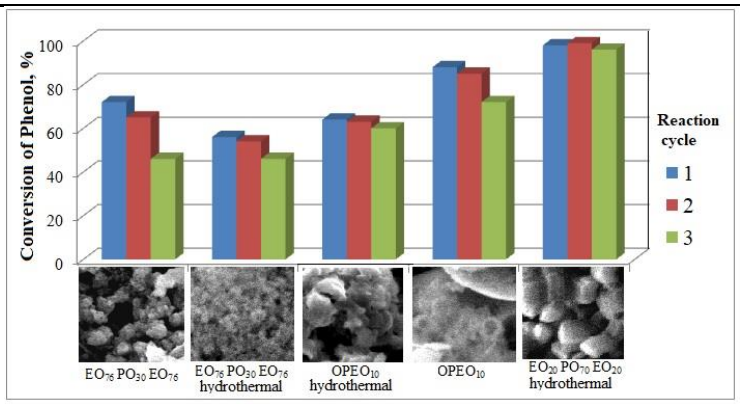

INTRODUCTION

In the last years, micelle-templated mesoporous silica materials have emerged as a solution for the development of many applications as catalysts or supports for pollutant removal, drug delivery systems, or biocompatible implants.[1-4] These applications demand the control of pore size, accessibility, morphology, stability and surface functionalization by various tailored synthesis strategies on surfactant packing and transformation of the liquid crystalline phase. Among the methods most used in the synthesis of mesoporous silica materials is soft templating in which a surfactant or amphiphilic block copolymer directs the mesoporous material synthesis by forming micelles

* Corresponding author: vpirvulescu@icf.ro

in solution, around which the silica precursor will be polymerized under hydrothermal conditions.[4] Despite the great working volume devoted to the preparation of mesoporous materials, the research carried out to understand the mechanism involved in their formation, is old and scarce.[5,6] The interactions between the surfactant and inorganic precursor determine the synthesis pathway, the mechanism of assembly and the class of the mesoporous materials obtained. Thus, the mesoporous materials can be prepared by electrostatic attraction manifesting in the case of ionic surfactants[7,8] or by hydrogen bounds established between the inorganic precursors and the surfactants.[8–12] In the last years, among the surfactants used to template nanostructured materials, polyethoxylated nonionic surfactants drew the attention of researchers due to their physico-chemical characteristics very interesting but also to their low-cost, reduced toxicity and biodegradability. Owing to their balanced hydrophilic-lipophilic character, ethoxylated surfactants present in aqueous solutions or in oil/water systems, are able to produce spectacular phenomena by small variations of concentration, temperature, immiscible phase ratio, or addition of electrolytes.[13-15] By changing both the hydrophobic (alkyl or alkylaril) and hydrophilic (polyethylene oxidic – PEO) chains, nonionic surfactants can cover a very wide range of polarities. As a function of chemical nature, concentration, and temperature, nonionic surfactants can produce various organized structures like spherical micelles, cylindrical, hexagonal, cubic, or lamellar aggregates. The assembly of inorganic polymerizable reactants on the surface of these structures allows obtaining materials with nanometric pores, without the use of swelling agents.[5,6,16] The obtained nanomaterials can have channeled disordered structures or well-ordered cubic, hexagonal, and lamellar arrangements of pores.

The neutral route to prepare mesoporous materials templated with polyethoxylated nonionic surfactants offers some advantages.[17] For example, the assembly can be carried out at neutral pH, at a relatively low reaction temperature (20 – 65 ºC). Also, the surfactant can be recovered by simple solvent extraction without affecting the surface areas and the pore size. In addition, the pore branching and especially, the complementarity textural porosity associated with the wormhole framework, can improve catalytic reactivity by facilitating access to the reactive sites in the framework. These characteristics make nonionic surfactants ideal to synthesize mesoporous materials. Among many mesoporous silicas obtained with nonionic surfactants, SBA-15 has attracted attention because of its large mesopores, stable pore walls and an interconnected 2D hexagonal mesostructure (p6mm).[18-20]

The mesoporous silica materials are well known as excellent catalyst supports due to their pores with tunable size, high specific surface area and ordered porous structure. The immobilization of heteroatoms on the surface of mesoporous silica frameworks can generate catalytically active sites. On the other hand, the impregnation of metal or metal oxide nanoparticles onto the mesopore surface is a very useful strategy to achieve high efficiency in the catalytic reaction. The obtained catalysts and photocatalysts, by immobilization of various metal species, proved a high activity in the oxidation of organic compounds[21-26] as phenol.[21, 24, 26] Among the metals immobilized on mesoporous silica, nickel has been less studied in oxidation reactions[22] or photocatalytic degradation of organic compounds.[23] In these reactions SBA-15 is among the most studied mesoporous silica as support with high surface area and ordered mesoporous structure to immobilization of various metals, and the obtained materials were used as catalysts[26] or photocatalysts.[27-31] Most of the photocatalysts contain Ti, single or associated with another active metal, supported on SBA-15, and were used in organic compounds degradation from water.[26-30] Photocatalysts that do not contain Ti have also been prepared, and an example is a series of mesoporous Ni_xCo_y/SBA-15 catalysts with different Ni/Co ratios. These materials showed high activity in benzyl alcohol conversion and selectivity to benzaldehyde.[31]

Recently has been revealed that NiO and TiO_2 semiconductor oxides have photocatalytic activity.[32] The band gap energy of NiO nanoparticles is 3.5 eV and these were utilized for the degradation of organic compounds.[32,33] It has been also proven that NiO-TiO_2 mixed oxides perform well as active photocatalysts in dyes degradation.[34]

Herein, novel micelle-mesoporous silicas were synthesized by nonionic surfactants as polydisperse ethoxylated octylphenol ($OPEO_{10}$) (Triton X-100) and ethylene oxide-propylene oxide-ethylene oxide (EO_{76}-PO_{30}-EO_{76}) and ($EO_{20}PO_{70}EO_{20}$) tri-block copolymers (Pluronic F68 and P123). The obtained mesoporous silica materials were characterized by X-ray diffraction at lower angles, scanning electron microscopy, transmission electron microscopy, N_2 adsorption-

desorption, UV-Vis and Infra-Red spectroscopy techniques, and were used as supports for Ni and Ti oxides immobilization. The structural and morphological properties of the obtained new materials were compared with those of SBA-15 mesoporous silica. In addition, catalytic and photocatalytic activity of the materials obtained by immobilization of metal (Ni, Ni/Ti) oxides were tested, with and without H_2O_2, for phenol and Brilliant Blue FCF dye oxidative degradation in a liquid phase. The effects of silica support on catalytic properties and supported nickel oxide on photocatalytic performances were evidenced.

RESULTS AND DISCUSSION

The synthesis route of mesoporous silicas was the electrically neutral assembly pathways based on the hydrogen-bonding interactions between the polyethylene oxide groups of surfactants and the tetraethylorthosilicate (TEOS). In the preliminary studies we used, as modeling agents of mesoporous silica structure, a series of $EO_x/PO_y/EO_x$ triblock copolymers ($PEO_{11}PPO_{16}PEO_{11}$-PL35, $PEO_{13}PPO_{30}PEO_{13}$ - PL64, $PEO_{20}PPO_{70}PEO_{20}$ – P123, $PEO_{76}PPO_{30}PEO_{76}$ - PF68) and ethoxylated octylphenol ($OPEO_{10}$) -Triton X-100. The used surfactants have different ethylene oxide (EO)/propylene oxide (PO) ratios and a hydrophilic-lyophilic balance (HLB) between 7 and 29. In the Triton X-100 surfactant molecule, the hydrophobic part is made up of the octylphenyl chain and the hydrophilic part, of PEO segments with a real average ethoxylation degree of about 10. The surfactants' characteristics are presented in Table 1. Pluronic triblock copolymers have a molecule consisting of a hydrophobic block of polypropylene oxide (PPO) framed by two hydrophilic blocks of polyethylene oxide (PEO), having the structure: EO_x-PO_y-EO_x. Pluronic triblock copolymers (EO_x-PO_y-EO_x) have a molecule formed by a hydrophobic block of polypropylene oxide (PO) surrounded by two hydrophilic blocks of polyethylene oxide (EO). Due to their amphiphilic nature, Pluronic molecules self-aggregate forming specific structures in the solvent, with the PEO groups orienting at the interface to avoid direct contact between the solvent and the insoluble block. Aqueous solutions of Pluronics offer a variety of phase behaviors and transitions between different states, determined by changes in the hydrophobicity mainly of the PPO block and to a lesser extent of the PEO block, under the influence of temperature or surfactant concentration. At concentrations lower than the critical micellar concentration (CMC), the copolymers exist in solution as individual monomers[35] and above the CMC, micellar aggregates appear. They have well-defined spherical shapes with the core consisting of the PPO block and surrounded by a crown in which the PEO blocks dominate. Depending on the concentration of the surfactant, self-aggregation can lead to the most different structural formations including mice of different shapes and sizes, complex structured microemulsions and liquid-crystalline phases.

Table 1

Characteristics of the surfactants used in the preparation of mesoporous silica materials

Surfactants	Commercial name	Molecular mass	(%) EO	HLB	CMC (M)
EO_{20} PO_{70} EO_{20}	Pluronic P123	5,800	30	8	4.4×10^{-6} [(a)]
EO_{13} PO_{30} EO_{13}	Pluronic PL64	2,900	40	15	4.8×10^{-4} [(a)]
EO_{11} PO_{16} EO_{11}	Pluronic PL35	1,900	50	19	5.3×10^{-3} [(a)]
EO_{76} PO_{30} EO_{76}	Pluronic PF68	8,400	80	29	4.8×10^{-4} [(a)] 7.1×10^{-4} [(b)]
$OPEO_{10}$	TritonX100	646.8	68	13.6	2.3×10^{-4} [(b)]

[(a)] CMC values from the literature.[36]

[(b).] CMC values determined in our laboratory by the ring method.

The concentration of the surfactant solutions used in our syntheses was higher than CMC for Triton X-100 and Pluronic P123 being 1×10^{-2} M and respectively 1.7×10^{-4} M. For all other Pluronics, the solutions had a surfactant concentration of 1.7×10^{-4} M, being smaller than CMC (see Table 1). The mesoporous silicas were synthesized at room temperature or by hydrothermal treatment and the obtained samples were compared with those prepared with a higher concentration of Pluronic P123 (2×10^{-3} M) in acidic conditions (pH=1.5) and hydrothermal treatment.

The chosen synthesis method, with polyethoxylated nonionic surfactants, highlight advantages such as the assembly of the reactant (TEOS), polymerizable on the surface of the micellar aggregates, both at neutral pH and at relatively low temperatures (20–65˚C). The obtained results showed that under these conditions (pH = 5 and 21˚C) the mesoporous silica materials were obtained only in the case of surfactants with higher EO percent (*i.e.*, Pluronic PF68 and TritonX100). They are in agreement with previous results obtained by the use of block copolymers in the synthesis of mesoporous silica, and attest that surfactants with shorter EO moieties form less ordered materials and the EO/PO ratio has a significant effect on the formation of the silica mesophase.[37] In the synthesis of mesoporous silica pH can influence both the silica condensation rate and the surfactant-water interaction. In our synthesis the silica condensation rate is about the same, at 1.5 and 5 values of pH, a result in accord with Zhao *et al*.[38] In acid media hydronium ions interconnect with oxygen atoms of EO by Coulombic interactions generating a more stable and ordered structure for the obtained mesoporous silica.

The particle shape and surface morphology of the synthesized samples were analyzed using scanning electron microscopy (SEM). Figure 1 shows a significant decrease in particle size for PF68 samples obtained by hydrothermal treatment and variation of their morphology.

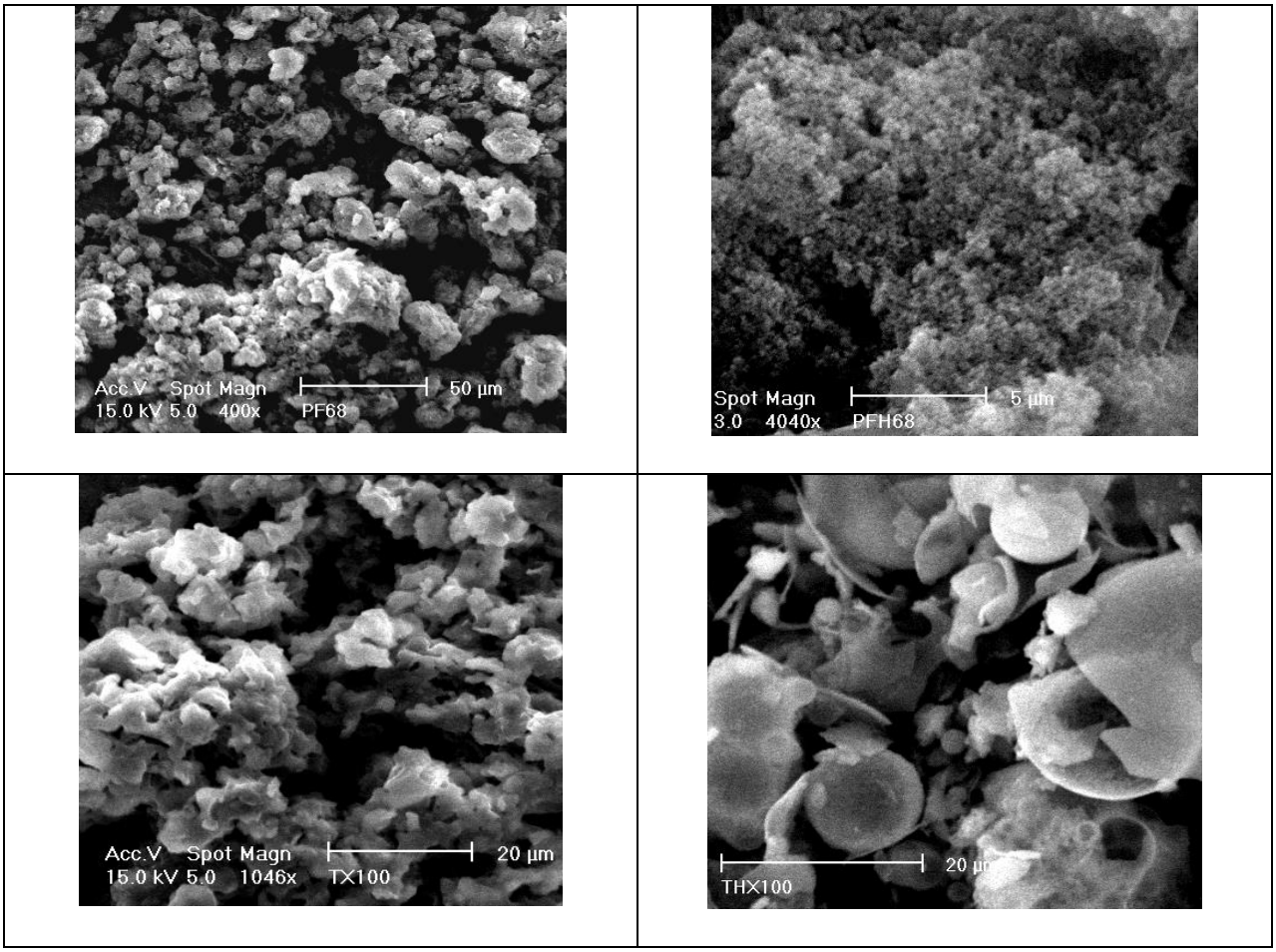

Fig. 1 – SEM images of mesoporous silicas obtained with Pluronic F68 and Triton X-100 surfactants at room temperature (samples PF68 and TX100) and by hydrothermal treatment (samples PFH68 and THX100).

A considerable change in morphology is also observed for the TXH100 sample obtained in an autoclave and by hydrothermal treatment compared to TX100 sample for which the aging was carried out at room temperature. In acid conditions and a higher concentration of P123 surfactant, typical for SBA-15 silica, a rod-like morphology was evidenced for the obtained sample (Fig. 2a). No effect of calcination on the morphology was evidenced for all the samples.

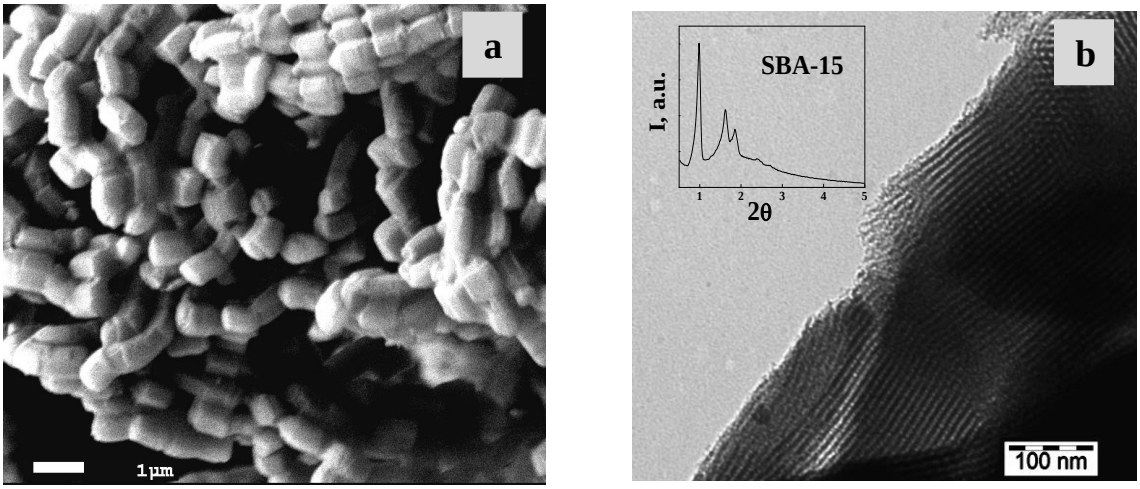

Fig. 2 – SEM (a) and TEM (b) images and X-Ray diffractogram (inserted figure) of SBA-15 sample.

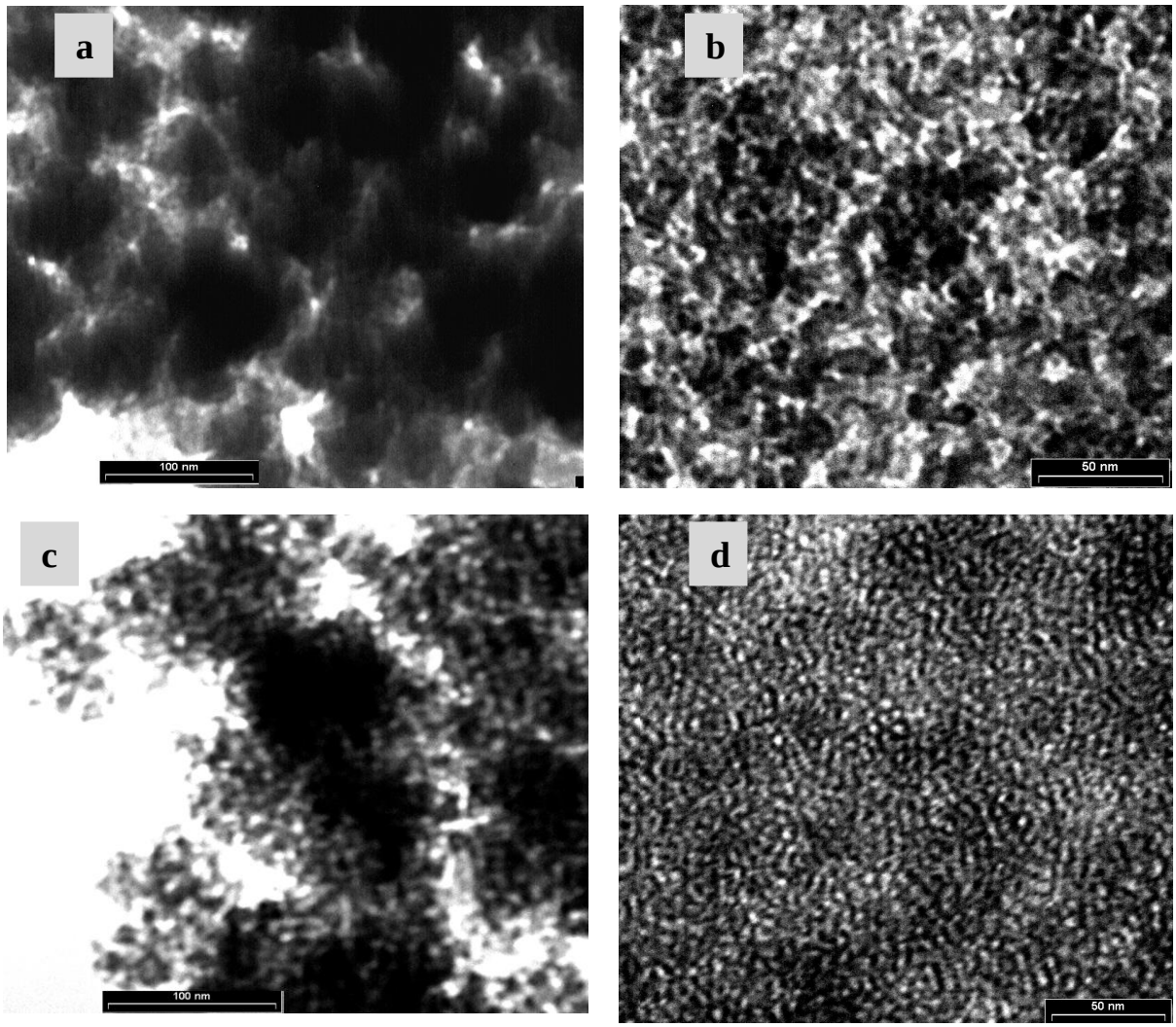

Fig. 3 – TEM images of PF68 (a), PFH68 (b, c) and TX100 (d) samples.

TEM micrographs (Fig. 2b) and X-Ray diffractogram (inserted in Fig. 2b) also confirm the hexagonal array of the ordered channels of our SBA-15 mesoporous silica. Though, the X-ray diffractograms at small angles of the other samples did not present peaks that indicate an ordered porous structure. TEM images from Fig. 3 show the presence of worm-like mesopores for PFH68

and TX100 samples. These images, coupled with results obtained by X-ray at small angles, suggest the possibility of local, but not in the bulk, order. TEM image from Fig. 3a indicates nanostructures formed by the packing of spherical micelles and confirms the formation of more disordered PF68 mesoporous silica. The mesopores were characterized by nitrogen sorption isotherms and pore size distribution (see Fig. 4)**.** All isotherms are typical for mesoporous silica (type IV). The H2 hysteresis loops of TX100 and PF68 samples evidence porous materials with pore size and pore shape not well defined. Unlike these silica materials, for SBA-15 H1 hysteresis typical for pores with narrow pore size distribution was obtained. A significant effect of the hydrothermal treatment on the adsorption-desorption isotherm can be seen in Fig. 4. Especially for the PFH68 sample, the adsorption-desorption isotherms indicate the formation of cavities probably due to agglomerations of surfactant molecules. For these samples was obtained a H4 hysteresis that show the presence of slit-shaped pores which lead to larger cavities in the case of sample PFH68. Pore size increased with surfactant molecule size and, in the case of the Pluronic surfactants (PF68 and P123), with degree of the hydrophobic polypropylene oxide block polymerization (lowest HLB value, see Table 1).

The highest pore volume and lowest surface area were obtained for the TX100 sample. High specific surface area was obtained for SBA-15 ordered mesoporous silica (894 m^2/g) and lower values for TX100 (682 m^2/g) and PF68 (542 m^2/g).

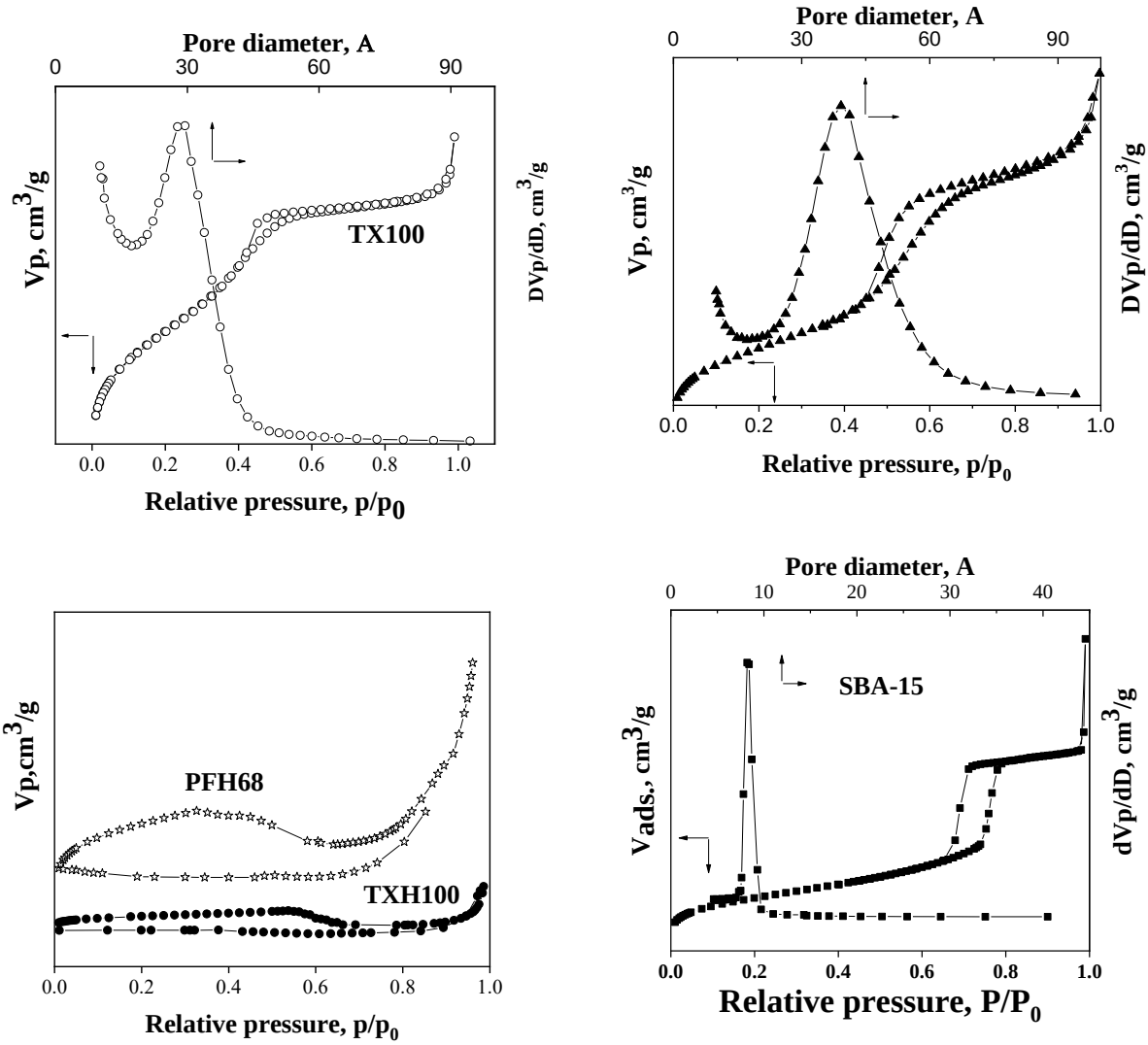

Fig. 4 – N_2 adsorption-desorption isotherms and pore size distribution of the mesoporous silica materials obtained with Triton X100 and PF68 surfactants without (samples TX100 and PF68) and by hydrothermal treatment (samplesTXH100 and PFH68) compared to SBA-15.

FTIR spectra of materials obtained with Triton X100 and PF68 surfactants, at room temperature (sample PF68) or hydrothermal treatment (samples TXH100 and PFH68) are analogs and typical for mesoporous silica. The variation of band intensity from about 3500 cm^{-1} shows the effect of hydrothermal treatment and calcination (samples marked with c) on silanols and physically adsorbed water from the silica surface. Thus, the higher silanol groups and adsorbed water molecules were evidenced for samples obtained by aging at room temperature. Comparing samples PFH68c and PF68c, can be observed that under hydrothermal treatment the number of silanol groups on the silica surface decreases significantly.

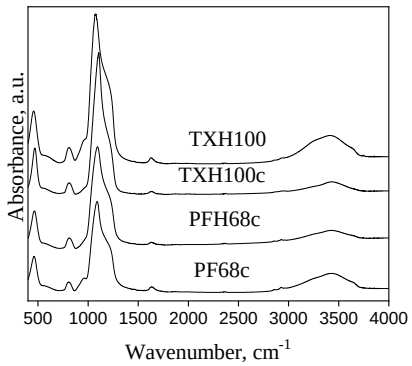

Fig. 5 – FTIR spectra of mesoporous silica materials obtained with Triton X100 and PF68 surfactants in presence and absence of the hydrothermal treatment before and after calcinations.

UV-Vis spectra of Ti/SBA-15 and Ni/Ti/SBA-15 samples indicates (Fig. 6) a wide absorption band in the UV range, suggesting their use in photocatalytic reactions carried out under conditions of irradiation with this light.

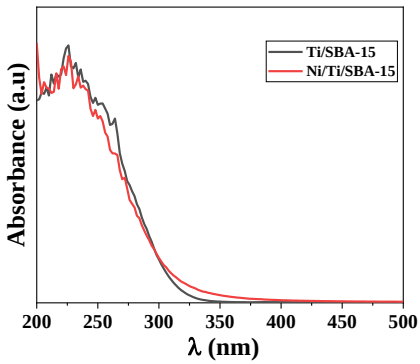

Fig. 6 – UV-Vis spectra of the Ti/SBA-15 and Ni/Ti/SBA-15 samples

The obtained materials were tested as a support for metals with catalytic or photocatalytic activity. A first test was carried out in the oxidation reaction of phenol with hydrogen peroxide. The catalysts used were obtained by immobilizing Ni nitrate on mesoporous silica oxides. The variation of conversion over time for the phenol oxidation in water was thus compared. The catalysts used were supported on silica obtained with or without hydrothermal treatment. The best conversion and stability were obtained for Ni/SBA-15 sample (Fig. 7). For the other samples, the conversion decreased as follows: Ni/TX100c > Ni/PF68c > Ni/TXH100c > Ni/PFH68c (Fig. 7).

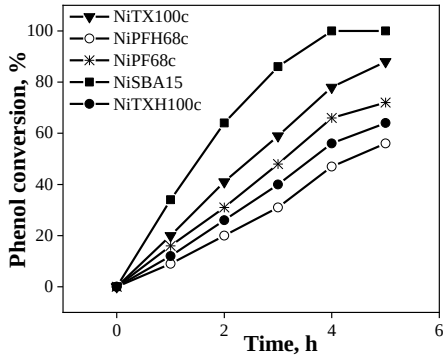

Fig. 7 – Variation of the phenol conversion with time for Ni/silica samples.

The difference between the obtained conversion values may be due to the structural and textural properties (specific surface area and pore shape). The high conversion obtained for Ni/SBA-15 is the result of the high specific surface area and the ordered porous structure that favors the mass transfer of the reactants to the surface-active centers. In the case of the other samples, the specific surface is lower and the shape of the pores is less favorable for mass transfer, especially in the case of samples obtained on supports synthesized by hydrothermal treatment (ex. PFH68). The greater number of silanol groups on the surface can favor the immobilization of Ni species and the increase of catalyst stability. The stability of these catalysts in the phenol oxidation reaction from aqueous solution was evaluated by isolating and reusing them in 3 successive reaction cycles. Figure 8 evidenced that the most stable catalyst is the one obtained by immobilizing nickel oxide on SBA-15 mesoporous silica. This support is often used in catalytic and photocatalytic reactions due to its stability, which is why we used it for comparison with the other supports synthesized with neutral surfactants. The decrease in conversion can be due to both changes in the support and leaching of nickel. Considering that the difference between the catalysts studied is

primarily due to the supports properties, we can explain the decrease in conversion as result of the support instability. The obtained results confirm that the more unstable supports were obtained without hydrothermal treatment.

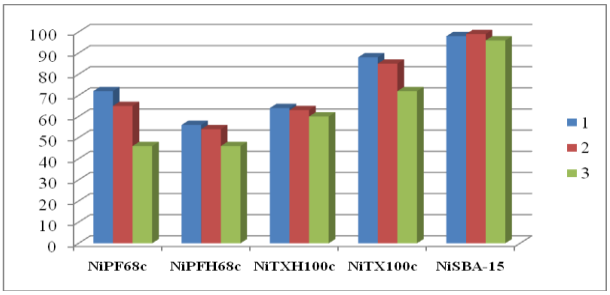

Fig. 8 – The variation of phenol conversion during three reaction cycles for the obtained catalysts.

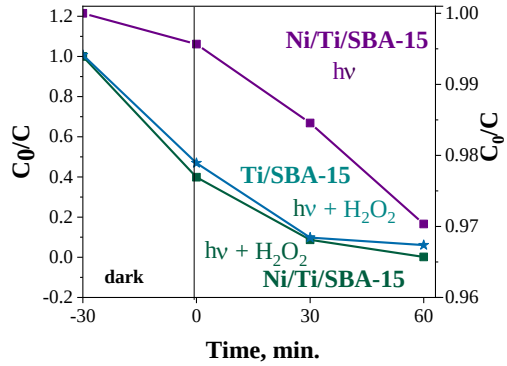

Fig. 9 – Degradation of phenol under UV light in presence and absence of H_2O_2.

Photocatalytic tests were carried out for the purpose of phenol degradation indicated insignificant conversions with the exception of the Ni/SBA-15 sample for which a degradation efficiency of 5% was obtained after 5 hours of irradiation. Instead, in the presence of hydrogen peroxide and irradiation, the degradation was 100% after only 1 hour of reaction (Fig. 9).

A similar effect of hydrogen peroxide was also observed for the NiTi/SBA-15 and Ti/SBA-15 samples in the case of the degradation of the Brilliant Blue FCF dye in water.

NiTi/SBA-15 and Ti/SBA-15 photocatalysts degraded Brilliant Blue FCF dye from water even in the absence of hydrogen peroxide (Fig. 10). The presence of nickel oxide near supported TiO_2 does not favor its activity. Decreasing of Ti/SBA-15 photocatalytic performance is result of higher band gap energy in the presence of NiO (3.46 eV). The rate constants (k) have been calculated for photocatalytic dye kinetics by measuring slopes on $\ln(C_0/C)$ against time. The degradation reaction of the Brilliant Blue FCF dye in the presence of NiTi/SBA-15 and Ti/SBA-15 photocatalysts was described by the Langmuir-Hinshelwood (L-H) model proving a pseudo-first-order kinetic for the photocatalytic process. The values obtained for kinetic constants were: 12.5×10^{-4} min^{-1} (with R^2=0.9859) for Ti/SBA-15 and 9.8×10^{-4} (R^2=0.9868) for NiTi/SBA-15, respectively

Both the catalytic and photocatalytic tests highlighted the effect of support and of immobilized metal oxide on the photocatalytic activity of the tested materials. It can be considered that the morphology of the supports obtained with TX100 and PF68 surfactants (Fig. 1) is not favorable for the illumination of the active centers, but this effect is insignificant compared to the photocatalytic inactivity of nickel oxide in the degradation of phenol.

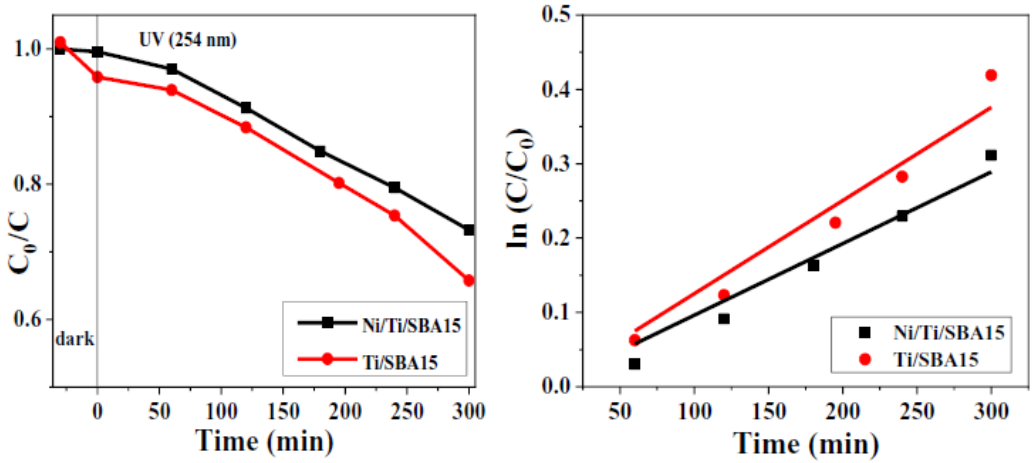

Fig. 10 – Variation of Brilliant Blue FCF dye photocatalytic degradation in time under UV (254 nm) and Plot of $\ln(C_0/C)$ *versus* time.

These results are also supported by some data from the literature[39] that indicate the need for a long irradiation time for the degradation of phenol in the presence of the nickel catalyst. The photocatalytic activity of nickel oxide was also lower in the case of dye degradation. The addition of hydrogen peroxide in the photocatalytic reactions, even in low concentration, favored the formation of •OH radicals, which are reactive oxygen species for the advanced degradation of phenol. This combined oxidation method represents an efficient solution for application se of the obtained materials as photocatalysts in phenol degradation, frequently found as pollutant in the wastewaters.

The previous studies that the rate of •OH radicals formation is higher than that of hydrogen peroxide decomposition.[40] The conversion products from the oxidative degradation of phenol, in the presence of hydrogen peroxide[40] or under UV radiation,[41] were analyzed by HPLC chromatography. The obtained products were: catechol, hydrochinone, resorcinol, maleic acid, fumaric acid, oxalic acid and acetic acid. Depending on the concentration of oxygenated water, the nature of the catalyst, the conditions and the reaction time, the concentration of advanced degradation products or the degree of mineralization varied.

EXPERIMENTAL

Materials

Tetraethylorthosilicate (TEOS) and PEO11PPO16PEO11 (L35), PEO13PPO30PEO13 (L64), PEO20PPO70PEO20 (P123) block copolymers were obtained from Sigma-Aldrich. PEO76PPO30PEO76 (Synperonic PE/F68), was obtained from Chemical & Polymer Group, England and Triton X-100 ($OPEO_{10}$) from Merck, Germany. The average ethoxylation degree of the sample determined by the NP-HPLC method as reported elsewhere[42] was 10.30 and the ethoxymer distribution ranged from 2 to 18. As metals precursors were used Titanium butoxide from Acros Organics and Nickel acetate from Sigma-Aldrich.

Preparation of mesoporous silicas

The mesoporous silica materials were synthesized at room temperature and by hydrothermal treatment as follows. The concentration of the surfactant solutions was 10^{-2} M for Triton X-100, 5×10^{-4} for P123 (for SBA-15 synthesis), higher than its critical micelle concentration (CMC) and 1.7×10^{-4} M for Pluronic F68 which was smaller than the CMC. The TEOS was added under stirring to surfactant dispersion in water. The final TEOS/H_2O/surfactant molar ratio was $1/56/1.7\times10^{-3}$. In the case of Triton X-100, the final molar ratio was $1/56/10^{-1}$ and for the synthesis of SBA-15 was $1/175.83/1.62\times10^{-2}$. The obtained sol-gels were aged under moderate stirring at 21°C for 15 hours or hydrothermal treated at 100°C. The obtained white solids were separated, dried in air dried at 80 °C and finally calcined at 550 °C.

Preparation of Ni/silica catalysts and Ni-Ti/SBA-15 photocatalysts

Ni/silica catalysts were obtained by impregnation of the mesoporous silica materials with aqueous solution of nickel acetate. The concentration of each solution was calculated taking into account the value of the determined impregnation capacity and the desired final concentration of nickel oxide (2.5 wt %).

After impregnation, the materials were dried for 24 hours at room temperature and at 80°C. Finally, the materials were calcined at 550°C for 8 hours in air. The obtained materials were named Ni/TX100c, Ni/TXH100c, Ni/PFH68c, Ni/PF68c and Ni/SBA-15. The synthesis of Ti/SB-15 (5% wt TiO_2) was presented in a previous article.[29] Ni/Ti/SBA-15 photocatalyst (2.5 wt % NiO) was obtained by impregnating the Ti/SBA-15 support with aqueous solution of nickel acetate through a procedure identical to the one described above.

Characterization of Materials

The samples were characterized by several experimental methods such as: X-ray diffraction, scanning electron microscopy (SEM), transmission electron microscopy (TEM), N_2 adsorption-desorption, IR spectroscopy. X-ray diffraction spectra were recorded on a Rigaku Ultima IV diffractometer by using CuK_α radiation (λ = 0.1541 nm). N_2 adsorption-desorption measurements were carried out at –196°C using a Micromeritics ASAP 2020 automated gas adsorption analyzer. The morphology of the sample was investigated by scanning electron microscopy (SEM) using a high-resolution microscope, FEI Quanta 3D FEG. The UV-Vis spectra were recorded on a PERKIN LAMBDA 35 Spectrophotometer. The average pore diameter was obtained from the desorption branch of the hysteresis curve using the Barrett–Joyner–Halenda (BJH) method.

Catalytic reactions

The obtained catalysts were tested in oxidation of phenol with hydrogen peroxide (molar ratio 1/3) in aqueous solution (1×10^{-2} M). The oxidation reactions were carried out in the thermostated glass microreactor (5 mL) with magnetic stirring at 30°C. Each reaction was carried out simultaneously in 5 microreactors, each using 0.05 g of catalyst. The contents of the micro-reactors were analyzed in turn at one-hour intervals. 3 mL of suspension was taken out and the catalyst separated from the suspension using a Millipore syringe filter. The variation of the phenol concentration was evaluated by measuring the UV-Vis absorbance of the isolated solution from the reaction mixture. After first reaction the catalyst powder was separated by centrifugation, dried and reused in two other reaction cycles.

Photocatalytic test

The photocatalytic reactions were carried out in quartz reactors, under magnetic stirring, at room temperature and in presence of UV radiation lamp (filter λ = 254 nm).[29] 9 mL of phenol aqueous solutions (6.4×10^{-4} M) was mixed, in dark conditions, with 6.8 mg of photocatalyst. After 30 minutes was introduced 0.5 mL of hydrogen peroxide aqueous solution (30%). The obtained mixture was irradiated with UV light.

Photocatalytic degradation of Brilliant Blue FCF from aqueous solutions (1×10^{-5} M) was carried out in quartz reactors, similar conditions 8 mL solution of dye and 1.5 mg of catalyst were used. At given irradiation times, 3 mL of suspension was taken out and the catalyst separated from the suspension using a Millipore syringe filter. In both types of test reactions the absorbance (*A*) of solution was measured by a Perkin Elmer Lambda 35 UV-Vis spectrophotometer. No analysis of the reaction products was performed.

CONCLUSION

Mesoporous silica materials were obtained in the presence of nonionic surfactants (Triton X100, Pluronic PF68 and 123), highlighting the effect of the surfactant nature and synthesis conditions on the structure and texture of the obtained supports. A significant role of pH and hydrothermal treatment was evidenced on the porous structure and its stability. The properties of the obtained silica supports did influence both the catalytic and photocatalytic properties of Ni/silica materials. The lower stability in catalytic oxidation was shown for catalysts with Ni supported on mesoporous silica obtained without hydrothermal treatment. Low photocatalytic activity was obtained both in the degradation of phenol and Brilliant Blue FCF dye. The association of UV light with small amounts of hydrogen peroxide determines a significant increasing of the phenol photocatalytic degradation.

REFERENCES

1. J. A. S. Costa, R. A. de Jesus, D. O. Santos, J. B. Neris, R. T. Figueiredo and C. M. Paranhos, *J. Environ. Chem. Eng.*, **2021**, *9*, 105259.
2. B. B. Galabova, *Trop. J Pharm. Res.*, **2021**, *20*, 1091–1100.
3. M. Ciobanu, L. Pirvu, G. Paun, S. Savin, B.- G. Albu, C. Munteanu, J. Pandele Cusu, I. Atkinson, D. Culita, G. Petcu and V. Parvulescu, *J. Drug Deliv. Sci. Technol.*, **2019**, *51*, 605–613.
4. T. Haynes, O. Bougnouch, V. Dubois and S. Hermans, *Microporous Mesoporous Mater.*, **2020,** *306*, 110400.
5. R. Guo and T. Q. Liu, *Colloids Surf. A: Physicochem. Eng. Asp.*, **1997**, *123-124*, 587-591.
6. P. Van Der Voort, M. Mathieu, F. Mees and E. F. Vansant, *J. Phys. Chem. B,* **1998**, *1102*, 8847-8851.
7. Z. A. ALOthman, *Materials*, **2012**, *5*, 2874-2902.
8. X. Zhang and K –Y Chan, *Chem. Mater.*, **2003**, *15*, 451-459.
9. A. M. Busuioc, V. Meynen, E. Beyers, M. Mertens, P. Cool, N. Bilba and E. F. Vansant, *Appl. Catal. A: Gen.*, **2006**, *312*, 153–164.
10. A. van Dillen, R. J. A. M. Terörde, D. J. Lensveld, J. W. Geus and K. P. Jong, *J. Catal.*, **2003**, *216*, 257–264.
11. Z. Dan and L. J. Hua, *Chinese Sci. Bull.*, **2013**, *58 (8)*, 879-883.
12. X. Zhang, F. Zhang and K. –Y. Chan, *Catal. Commun.*, **2004**, *5*, 749-753.
13. V. F. Vavsari, G. M. Ziarani and A. Badiei, *RSC Adv.*, **2015,** *5*, 91686–91707.
14. Z. Bagheryan, J.B. Raoof, R. Ojani and P. Rezaei, *Talanta*, **2014**, *119*, 24–33.
15. T. Kadoono and M. Ogura, *Phys.Chem. Chem. Phys.*, **2014**, *28*, 5495–5498.
16. S. Takahashi, Y. Ikkai, K. Sakamoto, C. R. Abreu and K. Aramaki, *J. Colloid Interface Sci.*, **2009**, *335*, 70-76.
17. K. Assaker, M.-J. Stébé and J.-L. Blin, *Colloids Surf. A: Physicochem. Eng. Asp.*, **2018**, *536*, 242-250.
18. D. Zhao, J. Feng, Q. Huo, N. Melosh, G. H. Fredrickson, B. F. Chmelka and G. D. Stucky, *Science*, **1998**, *279*, 548–552.
19. Z. Wang, R. Sun, P. Wang and W. Wang, *Microporous Mesoporous Mater.*, **2021**, *328*, 111491.
20. C. M. A. Parlett, H. Arandiyan, L. J. Durndell, M. A. Isaacsf, A. T. Lopez, R. J. Wong, K. Wilson and A. F. Lee, *Microporous Mesoporous Mater.*, **2022**, *329*, 111535.
21. S. Roy and D. Kumar Mondal, *Chem. Eng. Res. Des.*, **2022**, *182*, 120-132.
22. V. Parvulescu and B. L. Su, *Catal. Today*, **2001**, *69*, 315-322.
23. R. M. Mohamed, F. M. Ibrahim, K. Mori and H. Yamashita, *Stud. Surf. Sci. Catal.*, **2008**, *174*, 1255-1258.
24. M. Jourshabani, A. Badiei, Z. Shariatinia, N. Lashgari, G. M. Ziarani, *Ind. Eng. Chem. Res.*, **2016**, 55, 3900–3908.
25. J. Andas, F. Adam and I. Ab. Rahman, *Appl. Surf. Sci.*, **2014**, *315*, 154-162.
26. G. Almohammadi, C. O'Modhrain, S. Kelly, J. A. Sullivan, ACS Omega, **2020**, *5*, 791–798.
27. M. Filip, G. Petcu, E. Anghel, S. Petrescu, B. Trica, P. Osiceanu, N. Stanica, I. Atkinson, C. Munteanu, M. Mureseanu and V. Parvulescu, *Catal. Today*, **2021**, *366*, 10-19.
28. P. V. Suraja, Z. Yaakob, N. N. Binitha, M.R. Resmi and P.P. Silija, *Chem. Eng. J.*, **2011**, *176-177*, 265-271.
29. D. Negoescu, D. Culita, I. Atkinson, V. Bratan, S. Petrescu and V. Parvulescu, *Rev. Roum. Chim.*, **2021**, *66*, 287–293.
30. M. Ebrahimpour, S. K. Hassaninejad-Darzi, H. Z. Mousavi and A. Samadi-Maybodi, *Environ. Nanotechnol. Monit. Manag.*, **2022**, *18*, 100678.
31. R. Li, Y. Zhang, B. Xing, M. Huang, T. Wang, X. Hong, B. Zhou, B. Li, J. Ding and Q. Sui, *Microporous Mesoporous Mater.*, **2023**, *350*, 112407 .
32. A. Akbari, Z. Sabouri, H. A. Hosseini, A. Hashemzadeh, M. Khatami, M. Darroudi, *Inorg. Chem. Commun.*, **2020,** *115*, 107867.
33. D.M. Audi, *Res. J. Recent Sci*., **2017**, *6*, 16–22.
34. K. Indira, S. Shanmugam, A. Hari, S. Vasantharaj, S. Sathiyavimal, K. Brindhadevi, A. El Askary, A. Elfasakhany, A. Pugazhendhi, *Environ. Res.*, **2021**, *202*, 111647
35. K. Mortensen, *J. Phys. Condens. Matter*, **1996**, *8*, A103–A124.
36. M. Y. Kozlov, N. S. MeliK-Nubarov, E. V. Batrakova, A. V. Kabanov, *Macromolecules*, **2000**, *33*, 3305–3313.
37. H.P. Lin, C.-Y. Mou, *Acc. Chem. Res*., **2002**, *35*, 927–935.
38. D. Zhao, Q. Huo, J. Feng, B. F. Chmelka, G. D. Stucky, *J. Am. Chem. Soc.*, **1998**, *120*, 6024–6036.

39. T. T. Tri Dang, S. T. T. Le, D. Channei, W. Khanitchaidecha, A. Nakaruk, *Res. Chem. Intermed*., **2016**, *42*, 5961–5974.
40. K. M. Valkaj, O. Wittine, K. Margeta, T. Granato,.A. Katoviæ, S. Zrnèeviæ, *Pol. J. Chem. Technol.*, **2011**, *13*, 28–36.
41. M. Mureseanu, V. Parvulescu, T. Radu, M. Filip, G. Carja, *J. Alloys Compd*., **2015**, *648*, 864–873.
42. F. Anghel, M. Balcan, A. Voicu, M. Elian, *J. Chromatogr. A*, **1994**, *668*, 375–383.